

Susceptibility induced signal quenching in DCE-MRI is tissue dependent

Xin Li¹, Seymour Gahramanov², Charles S. Springer¹, William D. Rooney¹, and Edward A. Neuwelt²

¹Advanced Imaging Research Center, Oregon Health & Science University, Portland, Oregon, United States, ²Department of Neurology, Oregon Health & Science University, Portland, Oregon, United States

Introduction: Conventional gradient echo DCE-MRI protocols acquire data at short echo time (TE). During contrast reagent (CR) bolus passage, T₂* related MRI signal reduction (mainly due to susceptibility gradient introduced by CR) may not be negligible even with short TE, especially at ultra-high field. Using a sequential multi-session DCE-MRI data collection at 11.75T, we demonstrate that the T₂* signal loss in DCE-MRI is tissue dependent and most pronounced for tissues with low CR extravasation which transiently experience large intra-voxel susceptibility gradients.

Methods: MRI studies were performed with an 11.75 T instrument (Bruker, Billerica, MA). Coronal-equivalent head images from six male athymic nude rats were acquired four to ten weeks after U87 glioma cells were introduced into the right brain hemisphere. Each animal underwent three DCE-MRI sessions on two consecutive days with at least five hours gap between any two DCEs of the same animal to allow complete CR washout. The three GdDTPA-BMA (Omniscan) doses were 0.05 mmol/kg (after 1:2 dilution), 0.1 mmol/kg, and 0.2 mmol/kg. Each CR bolus was injected via a tail vein catheter, followed by ~ 0.24 mL saline flush. A quadrature volume RF transmit coil was used along with a surface receive RF coil placed on the animal's head. The three-slice fast-gradient-echo DCE-MRI sequence parameters were: TR/TE 25/1.39 ms, flip angle 20°, slice thickness 1.0 mm, rectangular FOV (5.12 x 2.56) cm², 128 read-out points with 50% phase encoding steps. These resulted in a 128 x 64 image matrix, and a 1.6 s temporal resolution. Matching ROI (across the three DCE studies) time-course data for the tumor, normal appearing brain (NAB), and temporalis muscle were obtained for each animal. The three dose DCE data of the same animal were modeled jointly and one set of parameters was extracted through simultaneously fitting the three enhancement curves. NAB data were modeled with a two-compartment (intravascular, extravascular) water exchange model (1) with the addition of a ΔR₂* relaxation term. For NAB, ΔR₂* was found to be better described by the quadratic relationship, ΔR₂* = a · [CR_p]² + b · [CR_p], than the commonly adopted linear one, ΔR₂* = r₂ · [CR_p], where r₂ is the CR transverse relaxivity. For tumor and muscle, a three-site (blood, interstitium, intracellular) model (1) was used. All tissue types employed the same empirical ΔR₂* expression except that for muscle and tumor, total voxel CR concentration ([CR]) instead of [CR_p] was used. The three adjustable parameters for NAB are blood volume fraction v_b, a (coefficient of quadratic term), and b (coefficient of linear term) of the ΔR₂* equation above. Four adjustable parameters were extracted for tumor and muscle: K^{trans} (CR transfer constant), v_e (extracellular extravascular volume fraction), a, and b. Here, instead of fitting v_b directly, a series of four parameter fittings were performed with different fixed v_b values. The fitted parameter set from the fixed v_b value that returns the least fitting error is reported.

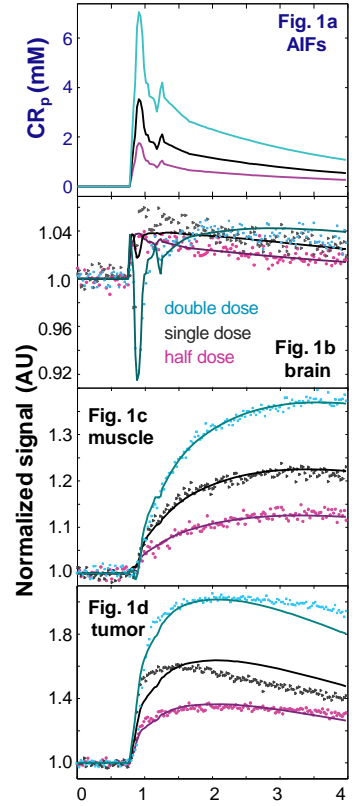
Results: Fig. 1a shows the [CR_p](t) plots, the arterial input functions (AIFs) for animal #6. The AIF time-course shape was determined from the half dose study, and its amplitude calculated using method described in (2). All AIF data points clearly occurring after the first-pass were further fitted with a bi-exponential decay function. Based on linear system assumptions, AIFs for single and double dose are set at peak heights two and four times of that of the half dose. Recursive tests reveal negligible T₂* contamination in our half dose AIFs. Fig. 1b shows the NAB data and fitting curves of the DCE studies of animal #6. Filled color symbols (off-pink: half dose; black: single dose; dark cyan, double dose) in 1b represent ROI time-course data; the color-matched curves display the best simultaneous fitting. For these curves, it is clear that the T₂* effect is appreciable, and is dominant during the CR first pass. Actually when all data points are weighted equally, data from double dose dominate the modeling when incorporating the T₂* effect. Fig. 1c and 1d show the 1b equivalent results for the muscle and tumor ROIs except that both are modeled to account for CR extravasation. For tumor, no apparent T₂* (signal reduction immediately following CR bolus injection) effect was observed for any animal of the study.

The Table summarizes the fitting results for all six animals studied. The v_b parameter for NAB is tight and consistent with other contrast-enhanced measurements (3). This supports the use of our empirical quadratic function for ΔR₂* modeling approach; for muscle and tumor with significant CR extravasation, the standard pharmacokinetic parameters values (eg. muscle v_e) were well within the normal range, suggesting that ΔR₂* plays a role closer to proportional signal reduction. An initial signal dip (as in NAB) was not observed using our sequence, and ΔR₂* effects are not as dominant in muscle and tumor as for NAB.

Discussion: Modeling T₂* effects in vivo with DCE-MRI data is feasible, especially when multiple CR doses are used. A simple quadratic ΔR₂* expression can empirically explain our data. Large intra-voxel susceptibility gradients exist at ultra-high field (B₀), especially for NAB which has an intact blood-brain barrier and maintains a large CR concentration gradient across blood vessels during CR first pass. In tissue with extravasating CR, where the intra-voxel [CR] gradient can be reduced even though the total voxel [CR] is higher, the apparent T₂* effect may not be apparent (no initial signal drop). However, for tissues with K^{trans} values ranging from 0.02 to 0.15, our results indicate that adding the T₂* term into the DCE-MRI modeling does not provide much extra information. In fact, the weaker fitting demonstrated for tumor ROI data suggests that other factors (e.g., water exchange, disproportionate signal quenching) may play a bigger role. However, it is necessary to incorporate some correction for ΔR₂* effects (even in single dose DCE-MRI) at ultrahigh field for tissues like NAB where large blood-parenchyma [CR] gradient is expected. The larger R₂* vs. [CR] nonlinearity (with GdDTPA-BMA) seen in this study than that of a recent 3.0 T study (4) using iron oxide nanoparticle contrast agent, further underscores the much stronger T₂* influence at ultrahigh field strength.

Grant Support: NIH: RO1-CA137488, RO1-EB00422, RO1- NS33618, RO1-NS34608, RO1-40801, NMSS RG 3168-A-1, and W. M. Keck Foundation.

Reference: 1. Li, Rooney, Springer, *Magn Reson Med*. 54:1351-9 (2005) [Erratum, 55:1217 (2006)]. 2. Li, Rooney, Várallyay, Gahramanov, Goodman, Tagge, Selzer, Pike, Neuwelt, Springer, *J. Magn. Reson.* 206: 190-199 (2010). 3. Schwarzbauer, Morrissey, Deichmann, Hillenbrand, Syha, Adolf, Noth, Hasse, *Magn. Reson. Med.* 37: 769-777 (1997). 4. Christen, Ni, Qiu, Schmiedeskamp, Bammer, Moseley, and Zaharchuk, *Magn. Reson. Med.* 000:000-000 (2012).



	K ^{trans} (min ⁻¹)	v _e	a (mM ⁻² s ⁻¹)	b (mM ⁻² s ⁻¹)	v _b
Brain	-	-	14.55 (± 3.84) ⁱ	2.26 (± 1.56)	0.025 (± 0.0015) ⁱ
muscle	0.046 (± 0.015)	0.095 (± 0.011) ⁱⁱ	11.42 (± 3.27)	4.59 (± 3.71) ⁱⁱⁱ	-
tumor	0.073 (± 0.012)	0.13 (± 0.01)	~ 0	1.13 (± 0.94) ⁱⁱⁱ	-

i: mean (± standard error); ii: assuming population fraction and volume fraction numerically equal; iii: only 2 out of 6 fittings result in non-zero b values for muscle; ii: 3 out of 6 tumor data result in non-zero b values.